PHYSICS

Spin vacuum switching

Eddie Ivor Harris-Lee[1], John Kay Dewhurst[1], Samuel Shallcross[2], Sangeeta Sharma[2,3]*

Ultrafast control over the magnetic orientation of matter represents a vital element of potential future spin-based electronics ("spintronics"). While physical mechanisms underpinning spin switching are established for picosecond time scales, we here present a physical route to magnetization toggle control, i.e., multiple switching events, at <100 femtoseconds. A minority spin current injected into a ferromagnet is shown to generate rapid depopulation of the minority channel below the ground-state Fermi level, creating a minority "spin vacuum" that then drives rapid charge redistribution from the majority channel and spin switching. We demonstrate that this mechanism reproduces many of the features of recent subpicosecond switching of ferromagnetic Co/Pt multilayers and provide simple practical rules for the design of materials via tailoring the electronic density of states to optimize spin vacuum control over magnetic order.

INTRODUCTION

A key problem of the "zettabyte era," in which the components of modern information technology consume more than 2% of global power generation, is the creation of energy-efficient and high-performance magnetic storage (*1*–*3*). Switching the magnetic orientation of matter on ultrafast (femtosecond) time scales and at low power thus represents not only a fascinating question of quantum solids but also one with profound technological implications. Low-dissipation all-optical and all-electronic approaches presently achieve subnanosecond switch times (*4*). Current-induced spin torque (*5*, *6*) is, however, believed to preclude subpicosecond switching times for ferromagnets (*7*, *8*).

Here, we propose switching of the magnetic moment of ferromagnetic systems at <100-fs times via injection of minority current. This, we show, generates ultrafast depopulation near the Fermi energy and the creation of a minority channel "spin vacuum," an intrinsically unstable situation that then results in rapid redistribution of charge from the majority channel and a reversal of the magnetic moment. In contrast to mechanisms of spin switching in which the moment rotates between majority and minority orientation, a slow process that fixes the resulting switching phenomena to the realm of picoseconds, in spin vacuum switching, the magnetization dynamics are strictly collinear and driven by the substantially faster processes of charge redistribution from one spin channel to another.

Recently, subpicosecond switching of magnetization in Co/Pt multilayers has been demonstrated, driven by ultrafast generation of spin current (*9*–*11*), and we show that the spin vacuum mechanism captures and explains key experimental facts of this ultrafast phenomenon, in particular, (i) spin reversal via a light-induced pulse of minority current, aided by heating, and (ii) return to original orientation with second current pulse of opposite polarity. Our ab initio approach, with an extension introduced here, allows us to provide simple practical rules for optimization of spin switching in magnetic materials, allowing design via tailoring the ground-state density of states.

Our work not only provides a conceptual framework for recent experiments but also demonstrates that the lower limit of switching time can be far shorter, on tens of femtosecond scale, and thus is limited only by the time scale on which spin current can be injected into the active component of the device. The uncovering of an ultrafast mechanism of both magnetization reorientation and reversible switching opens unexplored vistas in the control of magnetic order by light.

RESULTS

Femtosecond spin switching

The system sizes inherent in spin switching devices have, until now, prevented treatment by the ab initio approach. Here, we circumvent this by directly imposing a spin current on the "active" component of the device, for example, the free layer of a spin valve, bypassing the computationally expensive simulation of its full operation. Thus, rather than simulate the irradiation, generation of current, and subsequent switching of a spin valve, we simulate the essential spin dynamics of the switching process: the injection of a spin current into a ferromagnet, illustrated schematically in Fig. 1A. To this end we augment the fundamental equation of time-dependent density functional theory by an *SU*(2) potential, carefully tailored to generate a flow of current of specified polarity within the magnetic system; details of this approach are provided in Methods.

The spin dynamics resulting from injection of minority spin current into the ferromagnetic CoPt (Fig. 1B) reveal that above a critical threshold, this minority current induces complete reversal of the magnetization direction. (Note that this "minority spin current" always has spin polarity corresponding to the initial minority direction of the ferromagnet.) At no time during this ultrafast switching does moment perpendicular to the original magnetization axis develop: femtosecond scale magnetization switching without out-of-axis rotation (this is explicitly shown in section S7, where we plot the magnetization vector field in all three directions). To ensure that the conclusions that we draw (i.e., switching of spin orientation without rotation) are not an artifact of approximations used in the theory, which does not allow for local exchange-correlation spin torques (*12*, *13*), we have performed calculations that explicitly include such torques (see Methods for details) (*14*) and find exactly the same physics of switching without rotation (section S7).

We find that the critical threshold to induce magnetization reversal is material dependent (see Fig. 1C). We find that for CoPt, the threshold spin current required for switching is the right order of

[1]Max-Planck-Institut für Mikrostrukturphysik, Weinberg 2, 06120 Halle, Germany. [2]Max-Born-Institut für Nichtlineare Optik und Kurzzeitspektroskopie, Max-Born-Strasse 2A, 12489 Berlin, Germany. [3]Institute for Theoretical Solid State Physics, Free University of Berlin, Arnimallee 14, 14195 Berlin, Germany.
*Corresponding author. Email: geet1729@gmail.com

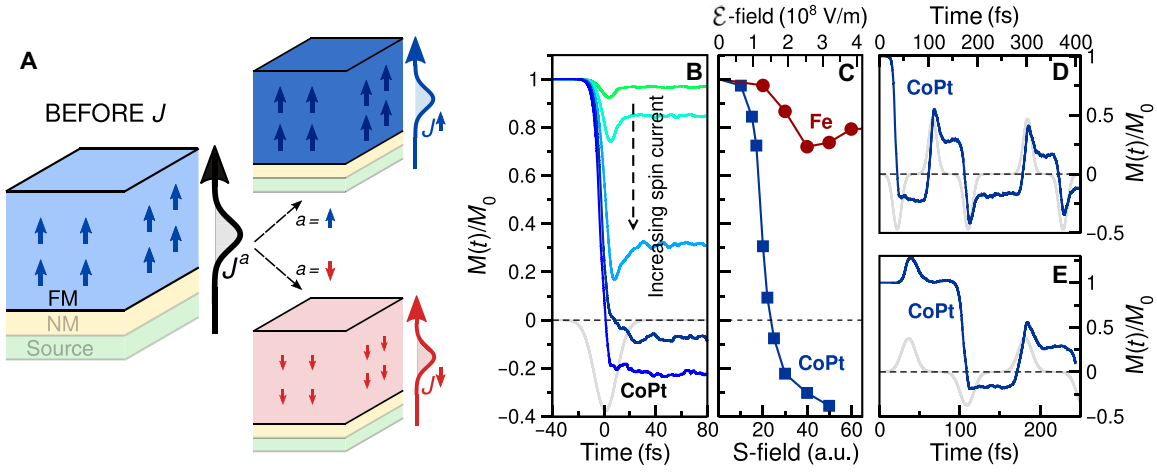

Fig. 1. Femtosecond magnetic switch. (**A**) Schematic of a device setup: A minority current ($J^{\downarrow}$, red) induces switching of the direction of the magnetic moment; a majority current ($J^{\uparrow}$, blue) leaves the magnetization direction unchanged but increases the magnitude of the moment slightly. The spin current could come from an external source via a conductive nonmagnetic spacer, but here, we directly impose the spin current saving the computationally prohibitive expense of calculation of the full device. (**B**) Above a critical amplitude of this minority current, the moment switches direction; note that the switching occurs on <20 fs. The gray lines represent the *SU*(2) effective potential (duration, 20.1 fs) that generates the spin current. (**C**) Final spin moment (expressed as a fraction of the ground-state moment M_0) as a function of the spin current potential maximum amplitude (S-field, atomic units) and the average spin electric field ($\mathcal{E} = -\frac{1}{c}\frac{dS}{dt}$; see Methods) for the spin current leading edge. While switching occurs for a critical value of S-field in CoPt, bcc Fe cannot be switched for any magnitude of the injected minority spin current. (**D**) Successive spin currents of opposite polarity induce successive reversals of the magnetization. (**E**) An initial injection of majority current does not cause reversal, neither does it inhibit the action of a subsequent minority spin current. Note that in [(B), (D), and (E)], a negative potential represents the injection of minority current, as defined relative to the initial state. a.u., Hartree atomic units.

magnitude for ultrafast spin currents that are generated by a laser pulse [see, for example, (*15*)]. Furthermore, switching is not observed in materials for which ultrafast switching is not known to exist, shown here with the example of body-centered cubic (bcc) Fe, highlighting the material predictive nature of the ab initio approach. A sequence of spin current pulses of opposite polarity induces a succession of magnetization reversals (Fig. 1D); an initial minority pulse induces magnetization reversal that can then be "toggled" back to its original state by a spin current pulse of opposite polarity.

Highlighting the crucial role that the polarity of the spin current plays in the switching mechanism, we see, in Fig. 1E, that an initial injection of majority current does not generate magnetization reversal, nor does it inhibit the action of a subsequent minority current pulse. These findings are in notable accord with recent experiments (*9*, *10*) in which spin current has been shown to induce subpicosecond switching in Co/Pt multilayers: (i) Switching is driven by minority current injection; (ii) magnetization reversal is not complete but rather some fraction of the ground-state moment, up to −0.1 M_0, and last, (iii) an initial pulse of majority spin current, created when GdFeCo is used to generate the minority current (*10*, *16*–*18*), neither leaves a lasting change to the magnetization nor inhibits further minority switching, exactly as seen in Fig. 1E. To better represent experimental situation, we have performed calculations for Co/Pt multilayers and CoPt, finding exactly the same physics of switching but for a slightly higher value of spin current (section S6).

Spin vacuum switching

To unveil the microscopic mechanism underpinning magnetization switching at the femtoscale, we now examine the dynamics as encoded in the density of states. The fundamental role of the current pulse is revealed by consideration of the dynamics in the absence of spin-orbit interaction, a constraint that precludes transitions between majority and minority channels. In this circumstance, a minority current is seen to depopulate the minority channel in a window down to ~2 eV below the Fermi energy (Fig. 2A), with corresponding increase above the Fermi energy. The substantial depletion of minority states below Fermi energy, which we term a minority channel spin vacuum, evidently represents a notably unstable electronic situation in which minority spin *d*-character holes are brought into energetic reach of the majority spin *d*-character electrons. Switching on spin-orbit coupling triggers rapid spin flips to correct this imbalance (Fig. 2C), leading to marked redistribution of charge between majority and minority channels and switching of the magnetization direction. This also explains the higher spin current required for switching in multilayers (section S6), where some of the Co atoms are further away from the high spin-orbit Pt atoms because of layered geometry.

The energy window ΔE_{vac}, indicated in Fig. 2 (A and B), plays a key role in the switching mechanism. Increasing the amplitude of the current pulse increases ΔE_{vac} (see section S1), and we find a simple microscopic rule for the onset of magnetic switching by current: The characteristic energy ΔE_{vac} must exceed the exchange splitting, $\Delta E_{vac} > \Delta E_{ex}$. This rationalizes the critical threshold of current seen in switching in CoPt (Fig. 1C). Examination of spin switching in a broad range of materials (section S2) reveals further rules for the design of spin switching materials. We find it highly advantageous for there to be a large density of available minority spin states in the energy domains marked (iii) and (iv) in Fig. 2, as well as a large density of majority states at (i). We also find it advantageous to have only a small density of available majority spin states at (ii): This may prevent undesirable minority to majority spin flips and help lock the reoriented state. Last, sufficient

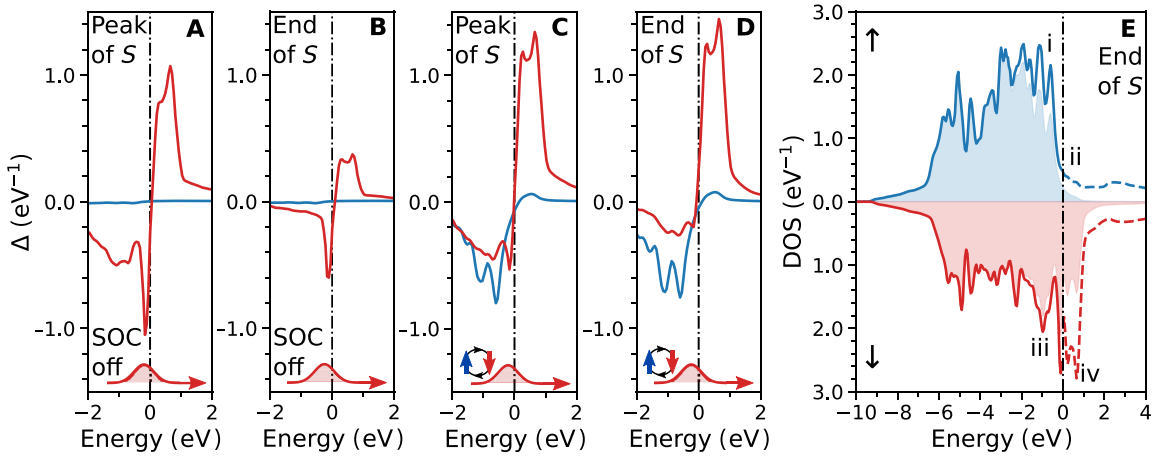

Fig. 2. Spin vacuum switching. (**A** and **B**) The change (Δ) in the density of states (DOS) induced by a minority spin current, shown at the maximum and end of the *SU*(2) driving potential *S*(*t*). While there is no change in the majority channel (blue), a substantial number of minority electrons (red) are excited across the Fermi energy (E_F), creating a "minority channel spin vacuum." Note that, here, spin-orbit interaction (SOC) is switched off. (**C** and **D**) Switching on SOC markedly changes the dynamics: The unstable spin vacuum is filled almost immediately by spin-orbit–induced spin flips from majority to minority. In contrast to (B) without SOC, the changes to the DOS mostly remain at the end. (**E**) The final DOS thus exhibits substantial reduction in the majority channel close to E_F, indicated by (i), with no corresponding increase above E_F (ii), while the minority also suffers almost no reduction below E_F (iii), as a result of excitation above E_F (iv). Overall, this results in a marked reduction in moment and, for sufficiently strong current generation, the reversal of the magnetic moment. Note that, here, the shaded regions denote occupied states, and the solid/dashed lines denote the ground-state DOS.

spin-orbit coupling is required (section S3) such that spin flips outpace the countervailing processes of spin vacuum relaxation, i.e., the relaxation of minority states.

We find this mechanism to be very robust against spin current depolarization, i.e., mixing of minority and majority channel spin currents. For the ferromagnetic CoPt system, we do not observe complete degradation of switching until the purity of the spin current falls below 20% (see section S4). Spin vacuum switching thus represents a highly robust mechanism of magnetization control.

Switching at finite temperature

The criterion for magnetization reversal by creation of a spin vacuum, $\Delta E_{vac} > \Delta E_{ex}$, implies that the reduction in exchange splitting ΔE_{ex} will allow satisfaction of the equality at lower current amplitude (and, hence, lower characteristic energy ΔE_{vac}). Recent experiments revealing subpicosecond spin switching have also noted that switching efficacy can be markedly improved by heating the target system (*9*, *10*, *17*, *18*). While a full treatment of temperature effects in transition metal magnets inevitably involves an account of the orientational disorder of local moments, the key physical property for the spin vacuum model, the *d*-band exchange splitting, can be captured by introducing a temperature-dependent parametrization of the exchange interaction (see Methods). In this approach, at zero temperature, the exchange splitting and magnetic moment take their equilibrium ground-state values, while at the Curie temperature, both fall to zero. The impact of finite temperature is, as in experiment, to facilitate spin switching (Fig. 3A), with magnetization reversal obtained for currents that cannot achieve any change at zero temperature. As expected, this is driven by the reduction in the exchange splitting (Fig. 3B; compared to Fig. 2E; also see section S1). For multiple switching events, in contrast, a mixed picture is revealed: While finite temperature can result in an improved fraction of recovered moment for the initial switching (i.e., the fraction of the ground-state moment after switching), multiple switching events rapidly lead to global demagnetization, shown in Fig. 3C.

DISCUSSION

We have presented a mechanism in which minority spin current generates femtosecond-scale reorientation of the magnetization direction, with further current pulses of alternating polarity yielding switching back and forth of the magnetic moment. The underlying microscopic mechanism involves the creation of a minority channel spin vacuum, a highly unstable depopulation of the minority channel below the ground-state Fermi level that triggers rapid spin-orbit–induced spin flip transitions from majority to minority, resulting in switching of the moment direction. The spin dynamics remain strictly collinear to the ground-state magnetization direction, with switching of the moment involving only the longitudinal degree of freedom of the magnetic moment.

This mechanism stands in notable contrast to spin-orbit torque (*6*) and spin-transfer torque (*5*), which allow spin switching on 50-ps or greater time scales and in which the exchange interaction addresses the purely rotational degrees of freedom of the magnetization. Recent experiments that unveil magnetization switching at 500 fs (*9*, *10*), however, present key features that are in common with the spin vacuum picture: (i) the crucial role of minority current, (ii) subpicosecond switching times and avoidance of critical slowing, and (iii) notable improvement in the efficacy of the switching mechanism at finite temperature.

While providing a compelling framework for understanding subpicosecond spin switching, the spin vacuum mechanism points toward unexplored functionality at few femtosecond times. With magnetization toggling driven by the ultrafast processes of spin-preserving charge dynamics and direct spin-orbit–induced spin flips, control over magnetization on times beating quantum decoherence (~5 fs) becomes

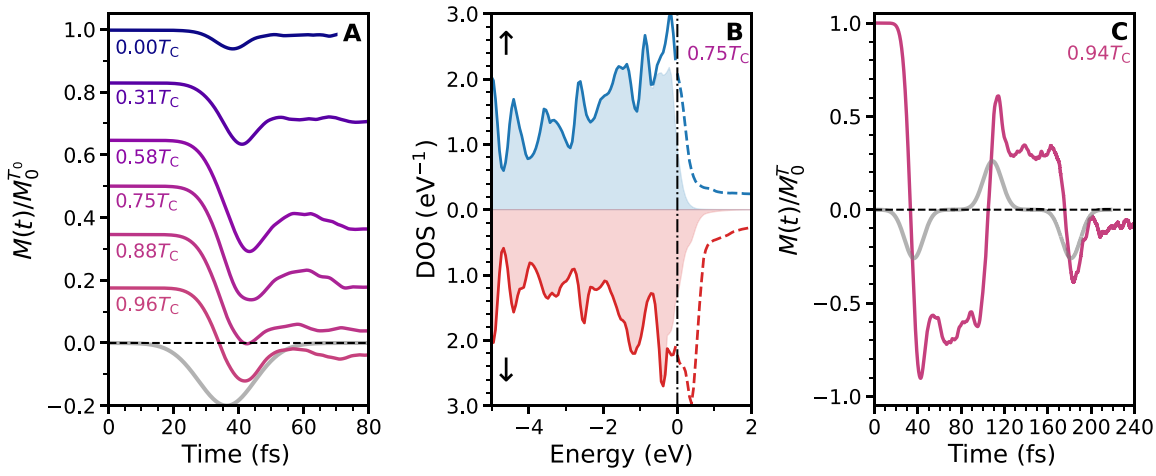

Fig. 3. Spin current toggling of magnetization direction at finite temperature. (**A**) Magnetization dynamics under action of a minority current pulse shown for temperatures $0 < T < 0.96\ T_C$. Temperature-induced reduction in magnitude of the magnetization allows for magnetization switching precluded at zero temperature, a phenomenon underpinned by the reduction in the exchange splitting at finite temperature. Shown in (**B**) is the DOS with reduced exchange splitting and occupations after the current pulse. (**C**) Successive pulses of opposite polarity toggle the magnetization with increased temperature, resulting in an increase in the fraction of the initial moment recovered in opposite orientation at the first switching event, but in faster onset of global demagnetization under multiple switching events, compare Fig. 1, D and E. [For comparison to Fig. 1C, here, $S = 10$ a.u. in (A) and (B) and 13 a.u. in (C).]

conceivable. With the present-day experimental drive toward laser control over current on few-femtosecond time scales, the key constraint to achieving this, which is the generation of ultrafast spin currents in a nanoscale device geometry, appears, in principle, solvable (*9*, *19*, *20*). Spin vacuum switching thus opens up promising avenues toward the long sought for femtosecond control over magnetic order.

METHODS

Underpinning time-dependent density functional theory is the Runge-Gross theorem (*21*), which establishes that the time-dependent external potential is a unique functional of the time-dependent density, given the initial state. On the basis of this theorem, a system of noninteracting particles can be chosen such that the density of this noninteracting system is equal to that of the interacting system for all times (*22*, *23*), with the wave function of this noninteracting system represented by a Slater determinant of single-particle orbitals. Dynamical evolution proceeds via the time-dependent Kohn-Sham equation

$$i\frac{\partial\phi_{j\mathbf{k}}(\mathbf{r},t)}{\partial t} = \left\{\frac{1}{2}\left[-i\nabla-\frac{1}{c}\mathbf{A}_{\mathrm{ext}}(t)\right]^2+\upsilon_{\mathrm{S}}(\mathbf{r},t)+\frac{1}{2c}\boldsymbol{\sigma}\cdot\mathbf{B}_{\mathrm{S}}(\mathbf{r},t) + \frac{1}{4c^2}\boldsymbol{\sigma}\cdot[\nabla\upsilon_{\mathrm{S}}(\mathbf{r},t)\times-i\nabla]\right\}\phi_{j\mathbf{k}}(\mathbf{r},t) \quad (1)$$

where $\phi_{j\mathbf{k}}(\mathbf{r}, t)$ are two-component Pauli spinor time-dependent Kohn-Sham orbitals with momentum $\mathbf{k}$ and state index j, $\mathbf{A}_{\mathrm{ext}}(t)$ is the external laser field, written as a purely time-dependent vector potential, $\boldsymbol{\sigma}$ are the Pauli matrices, $\upsilon_{\mathrm{S}}(\mathbf{r}, t) = \upsilon_{\mathrm{ext}}(\mathbf{r}) + \upsilon_{\mathrm{H}}(\mathbf{r}, t) + \upsilon_{\mathrm{xc}}(\mathbf{r}, t)$ is the Kohn-Sham effective scalar potential, and $\mathbf{B}_{\mathrm{S}}(\mathbf{r}, t) = \mathbf{B}_{\mathrm{ext}}(\mathbf{r}, t) + \mathbf{B}_{\mathrm{xc}}(\mathbf{r}, t)$ is the Kohn-Sham effective magnetic field. The external scalar potential, $\upsilon_{\mathrm{ext}}(\mathbf{r})$, includes the electron-nuclei interaction, while $\mathbf{B}_{\mathrm{ext}}(\mathbf{r}, t)$ is an external magnetic field that interacts with the electronic spins via the Zeeman interaction. The Hartree potential, $\upsilon_{\mathrm{H}}(\mathbf{r}, t)$ is the classical electrostatic interaction. Last, we have the exchange-correlation (xc) potentials, the scalar $\upsilon_{\mathrm{xc}}(\mathbf{r}, t)$, and the xc magnetic field, $\mathbf{B}_{\mathrm{xc}}(\mathbf{r}, t)$, which require approximation. In this work, we used the adiabatic local density approximation, constructed by functional derivative of energy with respect to magnetization, leading to the magnetization vector field being parallel to $\mathbf{B}_{\mathrm{xc}}$ everywhere and at each time. This implies that there is no local xc spin-torque at any time. To ensure that the physics is robust, we have also performed calculations with the source-free functional (*14*), which explicitly allows for and leads to spin-torques (*12*, *13*).

We calculate the magnetization density dynamics, $\mathbf{m}(\mathbf{r}, t)$, and thus the magnetic moment, $\mathbf{M}(t)$, directly from the expectation of the spin operator, $\boldsymbol{\sigma}$

$$\mathbf{m}(\mathbf{r},t) = \frac{1}{N_k}\sum_{j\mathbf{k}}^{\mathrm{occ}}\phi^{\dagger}_{j\mathbf{k}}(\mathbf{r},t)\ \ \boldsymbol{\sigma}\phi_{j\mathbf{k}}(\mathbf{r},t) \quad (2)$$

where $\phi_{j\mathbf{k}}$ is the spinor wave function with index j and momentum $\mathbf{k}$.

At the heart of our extended method, we add a time-dependent $SU(2)$ potential (corresponding to a non-Abelian gauge group) for spin currents (*24*, *25*) to the system Hamiltonian when we solve the time-dependent single-particle Schrödinger equation at various times. This is essentially a spin-polarized version of the $U(1)$ vector potential. To the vector potential–free Hamiltonian, H_0, we add a term

$$H_{\mathrm{S}}(t) = H_0(t) + \frac{i}{c}\sum_{p\mu}S_{p\mu}(t)\nabla_p\sigma_\mu \quad (3)$$

where $\frac{1}{c}$ is the coupling constant, p are Cartesian indices, μ are Cartesian indices plus a 0th index (to include the standard $U(1)$ vector potential in this single unified expression), and components of the linear momentum and spin vector operators appear because the conjugate operator to the spin current density is characterized by the tensor product $-i\ \nabla \otimes \boldsymbol{\sigma}$. The matrix functions $S_{p\mu}(t)$ are given the general form,

$$S_{p\mu}(t) = \sum_n g_n(t)\sin(\omega_n t+\phi_n)\mathcal{A}^n_p\mathcal{B}^n_\mu \quad (4)$$

where $g_n(t)$ is the nth envelope function (which is always a Gaussian here), ω_n is the frequency (0 here), ϕ_n is the phase shift ($\pi/2$ here), $\mathcal{A}_p$ is one part of a three-vector of real coefficients (amplitudes), and $\mathcal{B}_\mu$ is one of a four-vector of real coefficients. This form allows for arbitrary matrix functions $S_{p\mu}(t)$ including pure charge coupling ($\mathcal{B}_{\mu\neq 0} = 0$), pure spin coupling ($\mathcal{B}_0 = 0$), or mixtures thereof. A linear combination of Pauli matrices can be used to specify any spin matrix

$$\sigma = \mathcal{B}_\mu \sigma_\mu = \mathcal{B}_0\sigma_0 + \mathcal{B}_x\sigma_x + \mathcal{B}_y\sigma_y + \mathcal{B}_z\sigma_z, \quad (5)$$

so using $[-1, 0, 0, +1]$ for $\mathcal{B}_\mu$, we select the effective spin matrix

$$\sigma^{\text{minority}} = -\sigma_0 + \sigma_z = \begin{pmatrix} 0 & 0 \\ 0 & 2 \end{pmatrix} \quad (6)$$

for which any spinor with zero majority component is an eigenspinor. With this minority spin matrix in combination with the gradient operator ∇_z, we impose the "minority spin current potential" that we refer to here (Fig. 1, for example). The spin electric field ($\mathcal{E}$, Fig. 1C; i.e., the electric field for the minority electron channel minus the electric field of the majority electron channel) is calculated using $\mathcal{E} = -\frac{1}{c}\frac{dS}{dt}$. Overall, nonzero charge and spin current are both created. We note that in our calculations, the entire system experiences the same spin current potential simultaneously, and no overall spatial gradient in this potential is permitted, which is justified considering the typical experimental geometry and spin current (*9*). By this method, charge accumulation effects are excluded. We always take the initial majority (↑) magnetization to point in the +z direction of a Cartesian frame and minority (↓) spin to be anti-aligned along −z. Throughout, majority and minority refer to the initial net spin direction.

Finite temperature calculations

There exists an extension to density functional theory to account for finite temperature effects (*26*), but work to make it generally practical and accurate is ongoing (*27*). Instead, we simulate the relevant temperature effects through introduction of a scaling factor to the spin-dependent exchange potential. At each step of the self-consistent ground-state calculation, we calculate the values of $\mathbf{B}_{xc}(\mathbf{r})$ and $\mathbf{m}(\mathbf{r})$ in the regular way and then immediately modify them

$$\mathbf{B}_{xc}(\mathbf{r}) = \varsigma\mathbf{B}_{xc}(\mathbf{r}), \quad \mathbf{m}(\mathbf{r}) = \varsigma\mathbf{m}(\mathbf{r}) \quad (7)$$

where ς is the scaling factor. To simulate the finite temperature that would cause the magnetic moment to reduce to half of the zero temperature value, we calculate $\varsigma(\mathbf{M})$ (section S5) and choose the spin exchange scaling factor ς such that the ground-state moment is reduced by half. No temperature value enters into our method directly. The quoted temperatures are obtained by inserting the modified ground-state moment into the guideline equation,

$$\mathbf{M}(T)/\mathbf{M}(0) = (1 - T/T_C)^\beta \quad (8)$$

where we use the standard value, $\beta = 1/2$ (*28*). Although this exchange temperature method is not a complete time-dependent treatment of temperature, we find that it does successfully capture the most relevant finite temperature effects such as DOS exchange splitting reduction and total magnetic moment reduction.

Numerical details

We perform all of our calculations using the Elk code (*29*, *30*), with a full potential basis consisting of augmented plane waves plus local orbitals both above and below the Fermi level (*31*, *32*), providing maximum accuracy (*33*). We use the ab initio state-of-the-art fully noncollinear spin-dependent version (*30*, *34*) of time-dependent density functional theory with the time propagation algorithm detailed in (*30*), with a time step of 0.97 as. For bulk ferromagnetic CoPt, we have used a face-centered cubic cell with lattice parameter of 3.85. For multilayer geometry, we have used three layers of Co and three layers of Pt with an equivalent lattice parameter.

Supplementary Materials

This PDF file includes:

Sections S1 to S10
Figs. S1 to S12
Table S1

REFERENCES AND NOTES

1. A. Hirohata, K. Yamada, Y. Nakatani, I.-L. Prejbeanu, B. Dieny, P. Pirro, B. Hillebrands, Review on spintronics: Principles and device applications. *J. Magn. Magn. Mater.* **509**, 166711 (2020).
2. B. Dieny, I. L. Prejbeanu, K. Garello, P. Gambardella, P. Freitas, R. Lehndorff, W. Raberg, U. Ebels, S. O. Demokritov, J. Akerman, A. Deac, P. Pirro, C. Adelmann, A. Anane, A. V. Chumak, A. Hirohata, S. Mangin, S. O. Valenzuela, M. C. Onbaslı, M. d'Aquino, G. Prenat, G. Finocchio, L. Lopez-Diaz, R. Chantrell, O. Chubykalo-Fesenko, P. Bortolotti, Opportunities and challenges for spintronics in the microelectronics industry. *Nat. Electron.* **3**, 446–459 (2020).
3. A. Fert, P. Gruenberg, *The Nobel Prize in Physics* (2007); nobelprize.org.
4. A. V. Kimel, M. Li, Writing magnetic memory with ultrashort light pulses. *Nat. Rev. Mater.* **4**, 189–200 (2019).
5. D. C. Ralph, M. D. Stiles, Spin transfer torques. *J. Magn. Magn. Mater.* **320**, 1190–1216 (2008).
6. A. Manchon, J. Zelezny, I. Miron, T. Jungwirth, J. Sinova, A. Thiaville, K. Garello, P. Gambardella, Current-induced spin-orbit torques in ferromagnetic and antiferromagnetic systems. *Rev. Mod. Phys.* **91**, 035004 (2019).
7. K. Olejnık, T. Seifert, Z. Kaspar, V. Novak, P. Wadley, R. P. Campion, M. Baumgartner, P. Gambardella, P. Nemec, J. Wunderlich, J. Sinova, P. Kuzel, M. Muller, T. Kampfrath, Terahertz electrical writing speed in an antiferromagnetic memory. *Sci. Adv.* **4**, eaar3566 (2018).
8. K. Jhuria, J. Hohlfeld, A. Pattabi, E. Martin, A. Y. Arriola Cordova, X. Shi, R. Lo Conte, S. Petit-Watelot, J. C. Rojas-Sanchez, G. Malinowski, S. Mangin, A. Lemaıtre, M. Hehn, J. Bokor, R. B. Wilson, J. Gorchon, Spin–orbit torque switching of a ferromagnet with picosecond electrical pulses. *Nat. Electron.* **3**, 680–686 (2020).
9. J. Igarashi, W. Zhang, Q. Remy, E. Dıaz, J.-X. Lin, J. Hohlfeld, M. Hehn, S. Mangin, J. Gorchon, G. Malinowski, Optically induced ultrafast magnetization switching in ferromagnetic spin valves. *Nat. Mater.* **22**, 725–730 (2023).
10. Q. Remy, J. Hohlfeld, M. Verges, Y. Le Guen, J. Gorchon, G. Malinowski, S. Mangin, M. Hehn, Accelerating ultrafast magnetization reversal by non-local spin transfer. *Nat. Commun.* **14**, 445 (2023).
11. D. Afanasiev, A. V. Kimel, Ultrafast push for counterintuitive spintronics. *Nat. Mater.* **22**, 673–674 (2023).
12. J. K. Dewhurst, A. Sanna, S. Sharma, Effect of exchange-correlation spin–torque on spin dynamics. *European Phys. J. B* **91**, 218 (2018).
13. D. Hill, J. Shotton, C. A. Ullrich, Magnetization dynamics with time-dependent spin-density functional theory: Significance of exchange-correlation torques. *Phys. Rev. B* **107**, 115134 (2023).
14. S. Sharma, J. K. Dewhurst, A. Sanna, E. Gross, Source-free exchange-correlation magnetic fields in density functional theory. *J. Chem. Theory and Comput.* **14**, 1247–1253 (2018).
15. R. Rouzegar, A. Chekhov, Y. Behovits, B. Serrano, M. Syskaki, C. Lambert, D. Engel, U. Martens, M. Munzenberg, M. Wolf, G. Jakob, M. Klaui, T. Seifert, T. Kampfrath, Broadband spintronic terahertz source with peak electric fields exceeding 1.5 MV/cm. *Phys. Rev. Appl.* **19**, 034018 (2023).
16. G.-M. Choi, B.-C. Min, Laser-driven spin generation in the conduction bands of ferrimagnetic metals. *Phys. Rev. B* **97**, 014410 (2018).
17. S. Iihama, Y. Xu, M. Deb, G. Malinowski, M. Hehn, J. Gorchon, E. E. Fullerton, S. Mangin, Single-shot multi-level all-optical magnetization switching mediated by spin transport. *Adv. Mater.* **30**, e1804004 (2018).
18. J. Igarashi, Q. Remy, S. Iihama, G. Malinowski, M. Hehn, J. Gorchon, J. Hohlfeld, S. Fukami, H. Ohno, S. Mangin, Engineering single-shot all-optical switching of ferromagnetic materials. *Nano Lett.* **20**, 8654–8660 (2020).

19. T. Kampfrath, A. Kirilyuk, S. Mangin, S. Sharma, M. Weinelt, Ultrafast and terahertz spintronics: Guest editorial. *Appl. Phys. Lett.* **123**, 050401 (2023).
20. I. Ilyakov, A. Brataas, T. V. A. G. de Oliveira, A. Ponomaryov, J.-C. Deinert, O. Hellwig, J. Faßbender, J. Lindner, R. Salikhov, S. Kovalev, Efficient ultrafast field-driven spin current generation for spintronic terahertz frequency conversion. *Nat. Commun.* **14**, 7010 (2023).
21. E. Runge, E. K. U. Gross, Density-functional theory for time-dependent systems. *Phys. Rev. Lett.* **52**, 997–1000 (1984).
22. C. A. Ullrich, *Time-Dependent Density-Functional Theory* (Oxford Univ. Press, 2011).
23. S. Sharma, J. K. Dewhurst, E. K. U. Gross, in *Optical Response of Extended Systems using Time-Dependent Density Functional Theory* (Springer, 2014), pp. 235–257.
24. S. Pittalis, G. Vignale, F. G. Eich, U(1)×SU(2)gauge invariance made simple for density functional approximations. *Phys. Rev. B* **96**, 035141 (2017).
25. L. H. Ryder, *Quantum Field Theory* (Cambridge Univ. Press, 2013).
26. N. D. Mermin, Thermal properties of the inhomogeneous *electron gas*. *Phys. Rev.* **137**, A1441–A1443 (1965).
27. K. Burke, J. C. Smith, P. E. Grabowski, A. Pribram-Jones, Exact conditions on the temperature dependence of density functionals. *Phys. Rev. B* **93**, 195132 (2016).
28. N. Ashcroft, N. D. Mermin, *Solid State Physics* (Harcourt College Publishers, 1976).
29. J. K. Dewhurst, S. E. Sharma, *The Elk Code*, elk.sourceforge.net (2023).
30. J. K. Dewhurst, K. Krieger, S. Sharma, E. K. U. Gross, An efficient algorithm for time propagation as applied to linearized augmented plane wave method. *Comput. Phys. Commun.* **209**, 92–95 (2016).
31. D. J. Singh, *Planewaves Pseudopotentials and the LAPW Method* (Kluwer Academic Publishers, 1994).
32. E. Sjostedt, L. Nordstrom, D. J. Singh, An alternative way of linearizing the augmented plane-wave method. *Solid State Commun.* **114**, 15–20 (2000).
33. K. Lejaeghere, G. Bihlmayer, T. Björkman, P. Blaha, S. Blügel, V. Blum, D. Caliste, I. E. Castelli, S. J. Clark, A. D. Corso, S. de Gironcoli, T. Deutsch, J. K. Dewhurst, I. D. Marco, C. Draxl, M. Dułak, O. Eriksson, J. A. Flores-Livas, K. F. Garrity, L. Genovese, P. Giannozzi, M. Giantomassi, S. Goedecker, X. Gonze, O. Grånäs, E. K. U. Gross, A. Gulans, F. Gygi, D. R. Hamann, P. J. Hasnip, N. A. W. Holzwarth, D. Iuşan, D. B. Jochym, F. Jollet, D. Jones, G. Kresse, K. Koepernik, E. Küçükbenli, Y. O. Kvashnin, I. L. M. Locht, S. Lubeck, M. Marsman, N. Marzari, U. Nitzsche, L. Nordström, T. Ozaki, L. Paulatto, C. J. Pickard, W. Poelmans, M. I. J. Probert, K. Refson, M. Richter, G.-M. Rignanese, S. Saha, M. Scheffler, M. Schlipf, K. Schwarz, S. Sharma, F. Tavazza, P. Thunström, A. Tkatchenko, M. Torrent, D. Vanderbilt, M. J. van Setten, V. Van Speybroeck, J. M. Wills, J. R. Yates, G.-X. Zhang, S. Cottenier, Reproducibility in density functional theory calculations of solids. *Science* **351**, aad3000 (2016).
34. K. Krieger, J. K. Dewhurst, P. Elliott, S. Sharma, E. K. U. Gross, Laser-induced demagnetization at ultrashort time scales: Predictions of TDDFT. *J. Chem. Theory Comput.* **11**, 4870–4874 (2015).

Acknowledgments

Funding: E.I.H.-L., J.K.D., and S.Shar. thank the DFG for funding through project-ID 328545488 TRR227 (Project A04). S.Shar. would also like to thank the Leibniz Professorin program (P118/2021) for funding. Computations were performed on the HPC System Raven at the Max Planck Computing and Data Facility. **Author contributions:** J.K.D. and S.Shar. designed the project. E.I.H.-L. and J.K.D. wrote the code. E.I.H.-L. did the calculations. S.Shal. and E.I.H.-L. wrote the first version of the paper. All authors contributed to the final version of the paper and the interpretation of the results. **Competing interests:** The authors declare that they have no competing interests. **Data and materials availability:** All data needed to evaluate the conclusions in the paper are present in the paper and/or the Supplementary Materials. The code used in the manuscript is accessible at https://elk.sourceforge.io/.

Submitted 13 February 2024
Accepted 5 June 2024
Published 10 July 2024
10.1126/sciadv.ado6390